Proceedings of the 2021 IEEE
International Conference on Robotics and Biomimetics
December 27-31, 2021, Sanya, China

2021 IEEE International Conference on Robotics and Biomimetics (ROBIO) | 978-1-6654-0535-5/21/$31.00 ©2021 IEEE | DOI: 10.1109/ROBIO54168.2021.9739262

Manipulability-Oriented Configuration Transition Control of Continuum Surgical Manipulators Based on Velocity Polytopes

Yifan Wang, Yang Zheng, Longfei Wang, Bin Xu, and Kai Xu, *Member, IEEE*

***Abstract*—Continuum manipulators have gained popularity in surgical applications. During surgical operations, a continuum surgical manipulator can carry out tasks when partially inserted into a patient's abdominal cavity, enlarging the workspace of the manipulator. The inserted portion of the manipulator achieves different configurations, and a configuration transition control framework based on the resolved motion rate control was previously proposed. However, the inverse kinematics (IK) under the configuration transition framework sometimes fails due to the reduced kinematic ability in partially inserted configurations. This paper hence proposes to improve the IK performance of the configuration transition control using a manipulability measure based on velocity polytopes. The tasks are modified based on the constrained velocity polytopes that incorporate the configuration variable limits and the discontinuity on the configuration variable rates when a configuration transition is triggered. The task priority is reversed based on the ability of the continuum manipulator to perform a secondary task. Guided by the modified tasks, the manipulator moves towards the direction with higher manipulability and can possibly avoid the configuration variable limits or local minima. Numerical simulations were conducted to validate the proposed method, showing a higher success rate than the previous configuration transition control.**

I. Introduction

Continuum manipulators have attracted attention as a candidate for robot-assisted minimally invasive surgery (MIS), due to their dexterity, compliance, and design compactness [1]. Quite a few robotic surgical platforms have been developed with continuum manipulators adopted in their designs (e.g., the ones in [2-5]).

As investigated in [6], a multi-segment continuum surgical manipulator suffers from an unreachable volume inside their workspace when fully inserted into a patient's abdominal cavity through a trocar). Nevertheless, the continuum manipulator can perform tasks even while partially inserted, as shown in Fig. 1(a-c). Although the movement ability (a.k.a. the manipulability) may be reduced in these partially inserted configurations, they can enlarge the workspace of the manipulator, and hence extend the overall manipulability of the manipulator.

The configuration transition control during the insertion and extraction of a continuum manipulator was realized by a kinematics framework proposed previously [7], which solves the inverse kinematics (IK) under fully and partially inserted configurations in a unified way based on the resolved motion rate control. However, this framework fails from time to time while transforming among the partially inserted configurations due to the reduced manipulability.

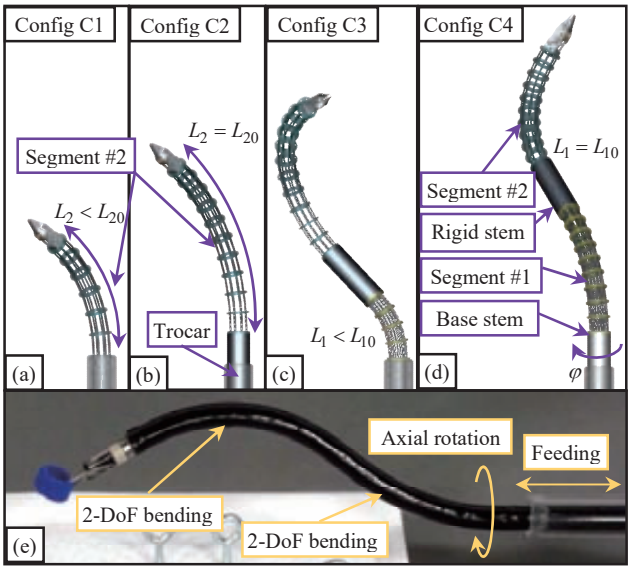

Figure 1. Different configurations of the continuum surgical manipulator: (a) the 1st configuration, (b) the 2nd configuration, (c) the 3rd configuration, and (d) the 4th (fully inserted) configuration; (e) the DoF allocation.

To characterize the manipulability of a manipulator, a manipulability measure has been proposed in [8], which describes the range of the end effector velocity using an ellipsoid whose principal axes are given by the singular vectors and singular values of the Jacobian matrix. This manipulability ellipsoid has been modified and used for manipulator configuration adjustment and trajectory planning. For instance, in [9], a measure of task compatibility is proposed based on the manipulability measure along the task direction. This compatibility measure is used in [10] to facilitate the execution of a trajectory tracking task, and is used in [11] to generate the optimal grasping pose for a dual-arm space robot. In [12], a constrained manipulability ellipsoid is proposed to select optimal grasp postures by penalizing the Jacobian with joint constraints and workspace obstacles.

*This work was supported in part by the National Key R&D Program of China (Grant No. 2017YFC0110800), in part by the Interdisciplinary Program of Shanghai Jiao Tong University (Grant No. YG2019QNB26), and in part by the National Natural Science Foundation of China (Grant No. 51722507).

Yifan Wang, Yang Zheng, Longfei Wang and Kai Xu are with the State Key Laboratory of Mechanical System and Vibration, School of Mechanical Engineering, Shanghai Jiao Tong University, Shanghai, 200240, China (e-mails: fan_tasy@sjtu.edu.cn, zzyy0608@sjtu.edu.cn, longfei.wang@sjtu.edu.cn, and k.xu@sjtu.edu.cn; corresponding author: Kai Xu).

Bin Xu is with the Department of Urology, Shanghai Ninth People's Hospital, School of Medicine, Shanghai Jiao Tong University, Shanghai, 200011, China (e-mail: chxb2004@126.com).

An alternative way to characterize the manipulability is the velocity polytope, which represents the actual feasible velocity rather than the approximation provided by the manipulability ellipsoid [13]. Moreover, since a polytope can be defined by a finite system of linear inequalities, joint and task space constraints can be easily incorporated into the polytope. The velocity polytope has been used to optimize the trajectories of robot manipulators [14, 15].

Inspired by the applications of manipulability in trajectory planning, this paper proposes a method to regulate the motion of the continuum manipulator to improve the success rate of the configuration transition IK. Constrained velocity polytopes are formulated by including the configuration transition limits and configuration variable limits. Based on the velocity polytopes, modified tasks are constructed such that the manipulator moves towards the direction with higher manipulability when the manipulability along the previous task direction becomes low. The task priority is reversed when the secondary task cannot be carried out well. The effectiveness of the proposed method is validated using numerical simulations.

The rest of this paper is organized as follows. Section II defines the configurations of the manipulator, while the proposed method is elaborated in Section III. Numerical simulations are presented in Section IV with the conclusions summarized in Section V.

II. Kinematics and Configuration Transition

A. Kinematics Nomenclature

The modeling of a single bending segment is shown in Fig. 2, while the nomenclatures are listed in Table. I. The kinematics of the manipulator can be referred to [7].

TABLE I. Nomenclature Used in the Kinematics Model

Symbol	Definition
t	Index of the segments. t = 1, 2.
j	Index of the configurations. j = 1, 2, 3, 4.
L_t, L_{t0}	Inserted length and the full length of the t^{th} segment.
L_r, L_{r0}	Inserted length and the full length of the rigid stem.
L_s, L_{s0}	Inserted length and the full length of the base stem.
θ_t	Bending angle of the t^{th} continuum segment.
δ_t	Bending direction angle of the t^{th} continuum segment.
φ	Axial rotation realized by the actuation unit.
$\mathbf{v}$, $\boldsymbol{\omega}$	Desired linear and angular velocity of the end effector.
$\boldsymbol{\psi}_{[j]}$	The configuration variable vector of the manipulator in the j^{th} configuration.
$\mathbf{J}_{[j]}$	The manipulator's Jacobian matrix in its j^{th} configuration.
$\mathbf{J}_{v[j]}$, $\mathbf{J}_{\omega[j]}$	Jacobian matrices of the tip linear velocity and angular velocity in the j^{th} configuration.

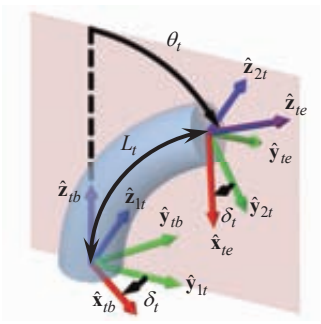

Figure 2. Kinematic modeling of the t^{th} bending segment.

B. Configuration Definition

The manipulator under investigation has two inextensible bending segments with a straight rigid stem in between, and the segment #1 is stacked on a base stem, as shown in Fig. 1(d). The manipulator is mounted onto an actuation unit, which provides rotation about and translation along its axis, as shown in Fig. 1(e). When an inextensible bending segment is partially inserted, the inserted portion kinematically possesses 3 Degrees of Freedom (DoFs): 2-DoF bending and 1-DoF length changing. The manipulator has 4 different configurations as follows.

- The 1st Configuration (C1): the segment #2 is partially inserted as shown in Fig. 1(a). The manipulator has 4 DoFs: axial rotation, length changing and 2-DoF bending of the segment #2. $\boldsymbol{\psi}_{[1]} = [\varphi\ \theta_2\ L_2\ \delta_2]^T$.
- The 2nd Configuration (C2): the rigid stem is partially inserted as in Fig. 1(b). The manipulator has 4 DoFs: axial rotation and feeding of the rigid stem, as well as 2-DoF bending of the segment #2. $\boldsymbol{\psi}_{[2]} = [\varphi\ L_r\ \theta_2\ \delta_2]^T$.
- The 3rd Configuration (C3): the segment #1 is partially inserted as in Fig. 1(c). The manipulator has 6 DoFs: 2-DoF bending of the segment #2, as well as axial rotation, length changing and 2-DoF bending of the segment #1. $\boldsymbol{\psi}_{[3]} = [\varphi\ \theta_1\ L_1\ \delta_1\ \theta_2\ \delta_2]^T$.
- The 4th Configuration (C4): the base stem is partially inserted as in Fig. 1(d). The manipulator has 6 DoFs: 2-DoF bending of the two bending segments with the axial rotation and translation of the base stem. $\boldsymbol{\psi}_{[4]} = [\varphi\ L_s\ \theta_1\ \delta_1\ \theta_2\ \delta_2]^T$.

C. Configuration Transition

The configuration transition is triggered when a length variable exceeds its limit during the insertion or extraction of the continuum manipulator. The triggering variables for the configuration transition are summarized in Fig. 3, and the strategies are briefly explained as follows.

- Between C1 and C2: the configuration with $L_2 = L_{20}$ in C1 is identical to that with $L_r = 0$ in C2. The transition from C1 to C2 is triggered when L_2 is updated longer than L_{20}, and. The overshoot of L_2 (excess value after one update) in C1 is set to L_r in C2:

$$L_{r[2]} = L_{2[1]} - L_{20}. \tag{1}$$

  The transition from C2 to C1 is triggered when L_r is updated less than 0. The overshoot of L_r (a negative value) in C2 is set to L_2 in C1:

$$L_{2[1]} = L_{r[2]} + L_{20}. \tag{2}$$

- Between C2 and C3: the configuration with $L_r = L_{r0}$ in C2 is identical to that with $L_1 = 0$ in C3. The transition from C2 to C3 is triggered when L_r is updated longer than L_{r0}. The overshoot of L_r in C2 is set to L_1 in C3:

$$L_{1[3]} = L_{r[2]} - L_{r0}. \tag{3}$$

  The transition from C3 to C2 is triggered when L_1 is updated less than 0. The overshoot of L_1 (a negative value) in C3 is set to L_r in C2:

$$L_{r[2]} = L_{1[3]} + L_{r0}. \tag{4}$$

- Between C3 and C4: the configuration with $L_1 = L_{10}$ in C3 is identical to that with $L_s = 0$ in C4. The transition from C3 to C4 is triggered when L_1 is updated longer than L_{10}. The overshoot of L_1 in C3 is set to L_s in C4:

$$L_{s[4]} = L_{1[3]} - L_{10}. \tag{5}$$

The transition from C4 to C3 is triggered when L_s is updated less than 0. The overshoot of L_s (a negative value) in C4 is set to L_1 in C3:

$$L_{1[3]} = L_{s[4]} + L_{10}. \tag{6}$$

After a configuration transition, the configuration variables other than the length variables are transferred from the previous configuration.

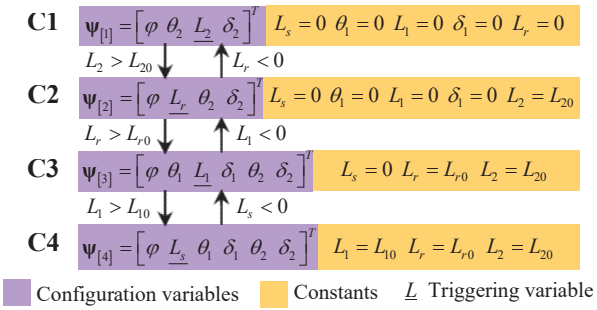

Figure 3. The variables and constants of the continuum manipulator and the transition conditions between the adjacent configurations.

III. Task Modification Based on Constrained Velocity Polytopes

While traversing multiple configurations to reach a target pose, gradient-based methods like resolved motion rate control may run into configuration limits that prohibit further reduction of the pose errors, or local minima such as converging to the target position under a different pose with a different orientation [7]. The failure is essentially because that the task of directly reducing the pose error is beyond the manipulability of the manipulator. To alleviate this problem, constrained velocity polytopes are used to characterize the manipulability of the manipulator along the desired task direction. Tasks are modified based on the polytopes.

A. Constrained Velocity Polytope

A d-dimensional polytope P can be represented as the convex hull of a finite set of points $X = \{x_1, \ldots, x_m\}$ in $\mathbb{R}^d$ (a.k.a. the V-representation):

$$P = \mathrm{conv}(X) \triangleq \{\sum_{i=1}^{m} \lambda_i x_i \mid \lambda_1,\ldots,\lambda_m \geq 0,\ \sum_{i=1}^{m} \lambda_i = 1\}. \tag{7}$$

Alternatively, P can be represented as the solution set of a finite system of linear inequalities (a.k.a. the H-representation), as in (8), with the condition that the solution set is bounded. The two representations of a polytope are equivalent and can be converted to each other.

$$P = \{\mathbf{x} \in \mathbb{R}^d \mid \mathbf{A}\mathbf{x} \leq \mathbf{b},\ \mathbf{A} \in \mathbb{R}^{m\times d},\ \mathbf{b} \in \mathbb{R}^m\}, \tag{8}$$

For the j^{th} configuration with n configuration variables, the configuration velocity polytope $Q_{[j]}$ is an n-dimensional polytope in the configuration space that contains all possible configuration velocities. For the i^{th} configuration variable in the j^{th} configuration $\psi_{i[j]}$, the velocity constraint is

$$\begin{cases} \dot{\psi}_{i[j]} \leq \min\{\dot{\psi}^{\max}_{i[j]}, (\psi^{\max}_{i[j]} - \psi_{i[j]})/\Delta t\} \\ \dot{\psi}_{i[j]} \geq \max\{\dot{\psi}^{\min}_{i[j]}, (\psi^{\min}_{i[j]} - \psi_{i[j]})/\Delta t\} \end{cases}, \tag{9}$$

where $\psi^{\max}_{i[j]}$ and $\psi^{\min}_{i[j]}$ denote the maximum and minimum configuration values, respectively; $\dot{\psi}^{\max}_{i[j]}$ and $\dot{\psi}^{\min}_{i[j]}$ denote the maximum and minimum allowed configuration velocities, respectively; Δt denotes the control loop time interval.

Moreover, consider the configuration transition driven by the insertion or extraction of the manipulator. When a configuration transition is triggered, similar task space twists may yield different directions of the configuration variable rates. This can cause the manipulator to oscillate back and forth between two configurations. Therefore, it is desirable to keep the direction of the length changing the same as that before the configuration transition, by constraining the length changing velocity as:

$$\begin{cases} \dot{L}_{i[j]} \geq k_L \dot{L}^{\min}_{i[j]}, \text{ during insertion} \\ \dot{L}_{i[j]} \leq k_L \dot{L}^{\max}_{i[j]}, \text{ during extraction} \end{cases}, \tag{10}$$

where $L_{i[j]}$ denotes the variable length in the j^{th} configuration and k_L is a coefficient that is set to 0.1 in this study. Writing (9) and (10) in a collective form gives the H-representation of the polytope $Q_{[j]}$ as:

$$\begin{bmatrix} \mathbf{I}_{n\times n} \\ -\mathbf{I}_{n\times n} \end{bmatrix} \dot{\boldsymbol{\psi}}_{[j]} \leq \begin{bmatrix} \dot{\boldsymbol{\psi}}^{\max}_{[j]} \\ -\dot{\boldsymbol{\psi}}^{\min}_{[j]} \end{bmatrix}, \tag{11}$$

where $\dot{\boldsymbol{\psi}}^{\max}_{[j]}$ and $\dot{\boldsymbol{\psi}}^{\min}_{[j]}$ are vectors of the maximum and minimum velocities of the j^{th} configuration, respectively. This definition indicates that $Q_{[j]}$ is an n-dimensional hyper-rectangle with 2^n vertices. The V-representation of $Q_{[j]}$ is hence given by its vertices arranged in a matrix as follows.

$$\mathbf{Q}_{[j]} = \begin{bmatrix} \dot{\psi}^{\max}_{1[j]} & \dot{\psi}^{\min}_{1[j]} & \cdots & \dot{\psi}^{\min}_{1[j]} \\ \dot{\psi}^{\max}_{2[j]} & \dot{\psi}^{\max}_{2[j]} & \cdots & \dot{\psi}^{\min}_{2[j]} \\ \vdots & \vdots & & \vdots \\ \dot{\psi}^{\max}_{n[j]} & \dot{\psi}^{\max}_{n[j]} & \cdots & \dot{\psi}^{\min}_{n[j]} \end{bmatrix}, \tag{12}$$

where the columns contain all possible velocity extremities.

The configuration space velocities can be transformed to task space velocities by the Jacobian matrix. Since the linear transformation of a polytope is also a polytope, the resulting task space velocities form a polytope that characterizes the manipulability. The velocity polytopes for the linear and angular velocities are given in the V-representation.

$$V_{[j]} = \mathrm{conv}(Col(\mathbf{J}_{v[j]}\mathbf{Q}_{[j]})),\ W_{[j]} = \mathrm{conv}(Col(\mathbf{J}_{\omega[j]}\mathbf{Q}_{[j]})), \tag{13}$$

where *Col*(**A**) represents the set consisting of all columns of the matrix **A**.

The velocity polytopes encapsulate all possible linear and angular velocities of the end effector that can be generated under the constraints in the configuration space. Based on the velocity polytopes, the manipulability of the manipulator along the task direction can be measured using a performance index that is similar to the transmission ratio proposed in [9]. Let a unit vector **u** denote the direction of the desired linear velocity, a scalar α is defined as the distance from the origin to the point where a ray along **u** intersects with a facet of the linear velocity polytope V. This intersection point $\alpha\mathbf{u}$ locates on one of the facets of V (including the edges and vertices). Since a facet of a polytope is a convex set, α must satisfy (14):

$$\alpha\mathbf{u} = \lambda_1\boldsymbol{\upsilon}_1 + \lambda_2\boldsymbol{\upsilon}_2 + (1-\lambda_1-\lambda_2)\boldsymbol{\upsilon}_3, \tag{14}$$

where

$$\alpha \ge 0, \quad \lambda_1 \ge 0, \quad \lambda_2 \ge 0, \quad \lambda_1+\lambda_2 \le 1, \tag{15}$$

And $\boldsymbol{\upsilon}_1$, $\boldsymbol{\upsilon}_2$, $\boldsymbol{\upsilon}_3$ are vertices of the triangular facet that contains $\alpha\mathbf{u}$. Therefore, α is obtained by finding the solution of (16) that satisfies (15):

$$\begin{bmatrix}\mathbf{u} & {}^k\boldsymbol{\upsilon}_3 - {}^k\boldsymbol{\upsilon}_1 & {}^k\boldsymbol{\upsilon}_3 - {}^k\boldsymbol{\upsilon}_1\end{bmatrix}\begin{bmatrix}\alpha & \lambda_1 & \lambda_2\end{bmatrix}^T = {}^k\boldsymbol{\upsilon}_3, \tag{16}$$

where ${}^k\boldsymbol{\upsilon}_1$, ${}^k\boldsymbol{\upsilon}_2$, ${}^k\boldsymbol{\upsilon}_3$ are vertices of the k^{th} triangular facet. The performance index α is the maximum linear velocity that the manipulator can generate along the direction **u**. Similarly, an index β is obtained based on W for angular velocity.

B. Modified Tasks

When the manipulator approaches the boundary of the translational or dexterous workspace, its manipulability largely decreases in certain directions, and the desired velocity might exceed the manipulability of the manipulator, which is indicated by reduction in the value of $\alpha_{[j]}$ or $\beta_{[j]}$. Enforcing the desired velocities in such situations will cause the manipulator to converge very slowly or towards a local minimum. Therefore, it is necessary to modify the desired twist tasks in order to restore the manipulability to reach the target. The modified tasks should guide the manipulator towards the direction where the manipulability is relatively high. Manipulability-oriented tasks are defined along the directions with high performance indices as follows:

$$\tilde{\mathbf{v}} = \|\mathbf{v}\|_2 \frac{\mathbf{v}^1_{\max[j]} + \mathbf{v}^2_{\max[j]}}{\left\|\mathbf{v}^1_{\max[j]} + \mathbf{v}^2_{\max[j]}\right\|_2}, \tilde{\boldsymbol{\omega}} = \|\boldsymbol{\omega}\|_2 \frac{\mathbf{w}^1_{\max[j]} + \mathbf{w}^2_{\max[j]}}{\left\|\mathbf{w}^1_{\max[j]} + \mathbf{w}^2_{\max[j]}\right\|_2} \tag{17}$$

where $\mathbf{v}^1_{\max[j]}$ and $\mathbf{v}^2_{\max[j]}$ denote the two vertices of the polytope $V_{[j]}$ with the largest distances from the origin, while $\mathbf{w}^1_{\max[j]}$ and $\mathbf{w}^2_{\max[j]}$ denote the two vertices of the polytope $W_{[j]}$ with the largest distances from the origin. These vertices correspond to the configuration variables moving towards the less constrained directions. Two vertices ($\mathbf{v}^1_{\max[j]}$ and $\mathbf{v}^2_{\max[j]}$ for linear velocity, $\mathbf{w}^1_{\max[j]}$ and $\mathbf{w}^2_{\max[j]}$ for angular velocity) are used to define the new task because the velocity polytopes are usually symmetric and the most distant vertices have the same distance from the origin. If the most distant vertices are opposite about the origin, only the one that is closer to the orientation of the original task is used.

The modified task is defined by combining the original task and the manipulability-oriented task as follows:

$$\mathbf{v}_m = \frac{k_\alpha\alpha_{[j]}\mathbf{v}/\|\mathbf{v}\|_2 + \eta_v\tilde{\mathbf{v}}}{k_\alpha\alpha_{[j]}/\|\mathbf{v}\|_2 + \eta_v}, \quad \boldsymbol{\omega}_m = \frac{k_\beta\beta_{[j]}\boldsymbol{\omega}/\|\boldsymbol{\omega}\|_2 + \eta_\omega\tilde{\boldsymbol{\omega}}}{k_\beta\beta_{[j]}/\|\boldsymbol{\omega}\|_2 + \eta_\omega}, \tag{18}$$

where k_α and k_β are constant normalizing factors to balance the magnitude of $\alpha_{[j]}$ and $\beta_{[j]}$. The modified tasks ensure that the manipulator mainly performs the desired task when $\alpha_{[j]}$ and $\beta_{[j]}$ are high, and the manipulability-oriented task gains more weight when the desired task cannot be carried out well. The manipulability-oriented tasks are multiplied by switching factors defined as

$$\eta_v = \begin{cases}0, & \text{if } e_P \le e_P^{thres}\\ 1, & \text{otherwise}\end{cases}, \quad \eta_\omega = \begin{cases}0, & \text{if } e_R \le e_R^{thres}\\ 1, & \text{otherwise}\end{cases}. \tag{19}$$

The switching factors block the manipulability-oriented tasks when the corresponding errors are less than the predefined thresholds. This enables the manipulator to stably converge to the target pose, other than drifting in the directions with higher manipulability [9].

C. Control Scheme

When an updated configuration variable violates its limit, its value is saturated at its limit, and the manipulator loses the corresponding DoF. To get the least-square solution of configuration velocities in such situations, dimension-reduced Jacobians [16] are used:

$$\tilde{\mathbf{J}}_{v[j]} = \mathbf{J}_{v[j]}\mathbf{H}_{[j]}, \quad \tilde{\mathbf{J}}_{\omega[j]} = \mathbf{J}_{\omega[j]}\mathbf{H}_{[j]}, \tag{20}$$

where $\mathbf{H}_{[j]}$ is the diagonal matrix for the j^{th} configuration with the diagonal elements as

$$h_{i[j]} = \begin{cases}0, & \text{if } \psi_{i[j]} \le \psi^{\min}_{i[j]} \text{ or } \psi_{i[j]} \ge \psi^{\max}_{i[j]}\\ 1, & \text{otherwise}\end{cases}. \tag{21}$$

As discussed in [17], the translational task and the rotational task have inconsistent metrics. Therefore, the linear and angular velocities are separately treated, with one of them chosen as the primary task and the other as the secondary task. The prioritized execution is handled by the null space projection as in [18]:

$$\dot{\boldsymbol{\psi}}_{[j]} = \mathbf{J}^+_{p[j]}\dot{\mathbf{x}}_p + [\mathbf{J}_{s[j]}(\mathbf{I} - \mathbf{J}^+_{p[j]}\mathbf{J}_{p[j]})]^+(\dot{\mathbf{x}}_s - \mathbf{J}_{s[j]}\mathbf{J}^+_{p[j]}\dot{\mathbf{x}}_p), \tag{22}$$

where $\dot{\mathbf{x}}_p$ and $\dot{\mathbf{x}}_s$ denote the primary and secondary tasks (selecting from $\mathbf{v}_m$ and $\boldsymbol{\omega}_m$), respectively; $\mathbf{J}_{p[j]}$ and $\mathbf{J}_{s[j]}$ denote the Jacobian of the primary and secondary tasks in the j^{th} configuration, respectively. $\mathbf{J}^+$ represents the Moore-Penrose pseudo-inverse of **J**. The priority of the tasks is determined by the capability of executing the secondary task, since the execution of the secondary task is constrained by the primary task. The capability for executing the secondary task is defined by a scalar γ as:

$$\gamma = \dot{\mathbf{x}}_s^T\mathbf{J}_{s[j]}\dot{\boldsymbol{\psi}}_{[j]}/\|\dot{\mathbf{x}}_s\|_2^2, \tag{23}$$

When $e_P \le e_P^{thres}$ or $e_R \le e_R^{thres}$, and γ is less than a predefined threshold k_γ, the secondary task is largely unsatisfied such that either the position or the orientation error cannot be further reduced, indicating a local minimum. In such situations, the priority is reversed (i.e., the secondary task becomes the primary task) for the following iterations.

IV. Numerical Simulations

The proposed method was verified in numerical simulations and compared to the previous configuration transition control. The configuration transition IK problem was solved for 500,000 test cases generated as follows. 125,000 poses were generated for each configuration by assigning random values to the configuration variables within the feasible ranges and calculating the forward kinematics. The 500,000 poses were randomly arranged to give the initial and the target poses for the test cases. The desired task velocities were obtained as follows:

$$\dot{\mathbf{x}} = \begin{bmatrix} \mathbf{v} \\ \boldsymbol{\omega} \end{bmatrix} = \begin{bmatrix} k_v \mathbf{e}_P \\ k_w \mathbf{e}_R \end{bmatrix} \tag{24}$$

The upper velocity limits for the prismatic and revolute configuration variables were 100 mm/s and π/3 rad/s, respectively. The time interval Δt is set to 50 ms. The error thresholds for convergence are 0.1 mm for position and 0.02 rad for orientation. The parameters used in the simulations are listed in Table II. All the simulations were carried out in MATLAB.

The proposed method achieved 99.68% success rate (1604 failed cases) on the test cases, showing an improved performance compared to the 94.44% success rate (27,820 failed cases) of the previous method. Two representative cases are analyzed as follows.

TABLE II. Parameters Used in Simulations

L_{10}	L_{20}	L_{r0}	L_g	L_{s0}	θ_1^{max}	θ_2^{max}
40 mm	60 mm	20 mm	20 mm	150 mm	π/2	2π/3
k_v	k_w	k_α	k_β	k_γ	e_P^{thres}	e_R^{thres}
10	8	50	100	0.01	10 mm	0.3 rad

A. Case Study #1

This case starts in C1 with the target pose in C3 whose position is lower than the initial position in the **z**-direction. The previous method was stuck at the boundary between C1 and C2, as indicated by the red arrow in Fig. 4(a). In C1, reducing the position error requires extending and bending the segment #2 until the manipulator enters C2. However, in C2, the segment #2 has already bent to the maximum angle, and the manipulator has to extract the rigid stem to reduce the position error, leading the configuration back to C1. By contrast, the proposed method recognized the low manipulability along **v** from the significant reduction of α in C2, as shown in Fig. 4(b). Since the manipulator entered C2 from C1 and θ_2 was close to its limit, the linear velocity polytope was constrained in the negative **z**-direction, and the manipulability-oriented task pointed upward, as shown in Fig. 4(a). The modified task guided the manipulator to extend the rigid stem and enter C3 to converge to the target pose, even though the position error temporarily increased, as shown in Fig. 4(c).

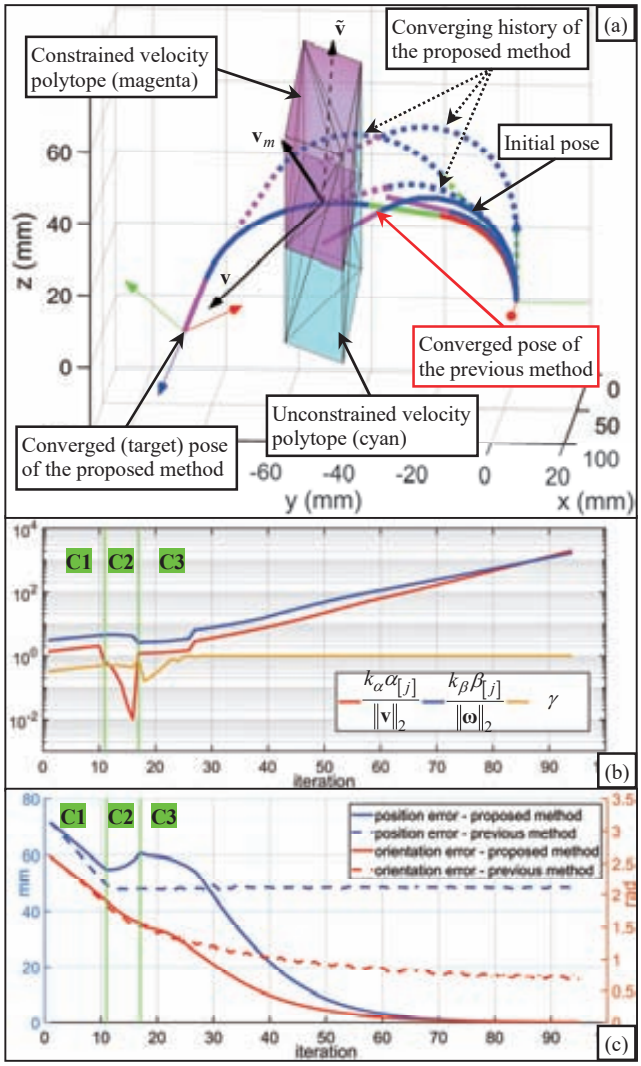

Figure 4. Case #1: (a) visualization of the converging history with the linear velocity and the polytope; (b) plot of the position and the orientation errors; (c) plot of the task-oriented manipulability performance indices.

B. Case Study #2

The second case starts in C2 with the target pose in C3. The previous method from [7] eventually converged to a pose that is still in C2 but the position was very close to the target position, as indicated by the red arrow in Fig. 5(a). This was because that the linear velocity was the primary task in the previous method, and the manipulator chose to first reduce the position error at the expense of not reducing enough orientational error. The manipulator converged to the position in C2 since the target position lies in the intersection of the translational workspaces of C2 and C3. However, the dexterous workspaces of C2 and C3 are not connected at this position, and the orientation cannot be reached without increasing the position error, which is not inherently possible in the previous method. By contrast, in the proposed method, when the manipulator converged to the target position in C2, the reduction of γ indicated that the desired angular velocity was not satisfied, as shown in Fig. 5(b). Therefore, the angular velocity was chosen as the

primary task, and the manipulator converged to the target pose in C3 with a slight increase in the position error, as shown in Fig. 5(c).

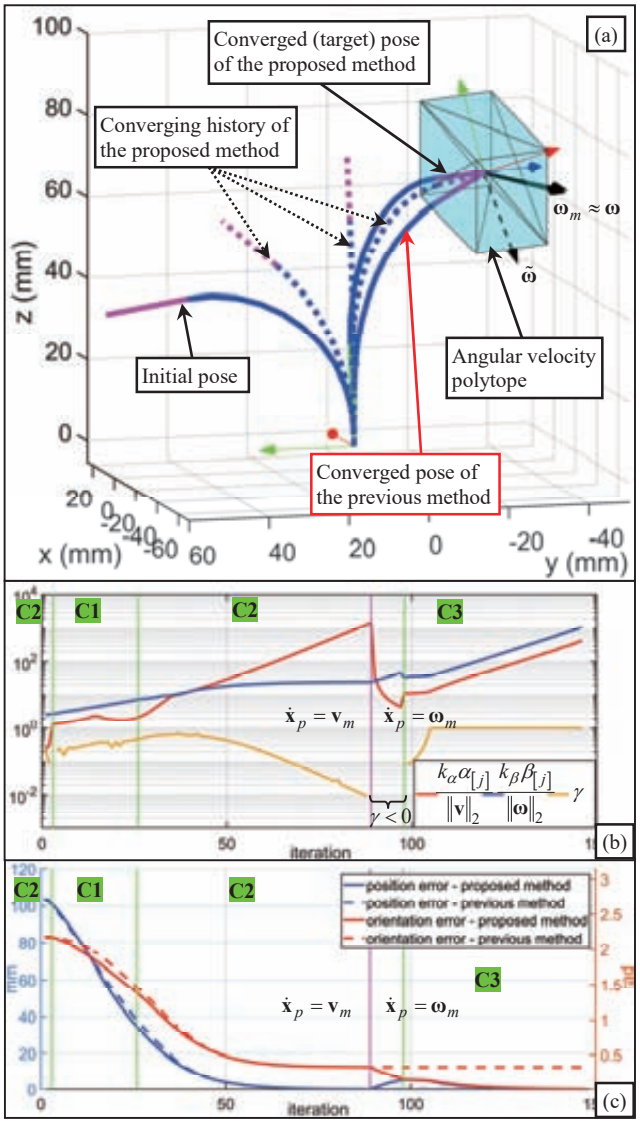

Figure 5. Case #2: (a) visualization of the converging history, with the angular velocity and the polytope; (b) plot of the position and the orientation errors; (c) plot of the task-oriented manipulability performance indices.

V. Conclusion

To address the problem that the configuration transition IK for continuum manipulators fails occasionally, this paper proposes to modify the velocity tasks using velocity polytope based manipulability measure. Constrained velocity polytopes are formulated, incorporating the configuration variable limits and the discontinuity on the configuration variable rates when a configuration transition is triggered. Using the velocity polytopes, modified tasks are constructed such that the manipulator moves towards the direction with higher manipulability. The task priority is reversed when the secondary task cannot be carried out with a characterizing variable value higher than a threshold. The proposed method is compared to the previous configuration transition control method via numerical simulations, showing a 94.24% decrease in the failure rate (0.32% vs. 5.56%).

References

[1] J. Burgner-Kahrs, D. C. Rucker, and H. Choset, "Continuum Robots for Medical Applications: A Survey," *IEEE Transactions on Robotics,* vol. 31, no. 6, pp. 1261-1280, Dec 2015.

[2] J. Ding, K. Xu, R. Goldman, P. K. Allen, D. L. Fowler, and N. Simaan, "Design, Simulation and Evaluation of Kinematic Alternatives for Insertable Robotic Effectors Platforms in Single Port Access Surgery," in *IEEE International Conference on Robotics and Automation (ICRA)*, Anchorage, Alaska, USA, May 3-8 2010, pp. 1053-1058.

[3] P. E. Dupont, J. Lock, B. Itkowitz, and E. Butler, "Design and Control of Concentric-Tube Robots," *IEEE Transactions on Robotics,* vol. 26, no. 2, pp. 209-225, April 2010.

[4] Y.-J. Kim, S. Cheng, S. Kim, and K. Iagnemma, "A Stiffness-Adjustable Hyperredundant Manipulator Using a Variable Neutral-Line Mechanism for Minimally Invasive Surgery," *IEEE Transactions on Robotics,* vol. 30, no. 2, pp. 382-395, April 2014.

[5] K. Xu, J. Zhao, and M. Fu, "Development of the SJTU Unfoldable Robotic System (SURS) for Single Port Laparoscopy," *IEEE/ASME Transactions on Mechatronics,* vol. 20, no. 5, pp. 2133-2145, Oct 2015.

[6] K. Xu, J. Zhao, and X. Zheng, "Configuration Comparison among Kinematically Optimized Continuum Manipulators for Robotic Surgeries through a Single Access Port," *Robotica,* vol. 33, no. 10, pp. 2025-2044, Dec 2015.

[7] S. a. Zhang, Q. Li, H. Yang, J. Zhao, and K. Xu, "Configuration Transition Control of a Continuum Surgical Manipulator for Improved Kinematic Performance," *IEEE Robotics and Automation Letters,* vol. 4, no. 4, pp. 3750-3757, Oct 2019.

[8] T. Yoshikawa, "Manipulability of Robotic Mechanisms," *International Journal of Robotics Research,* vol. 4, no. 2, pp. 3-9, June 1985.

[9] S. L. Chiu, "Task Compatibility of Manipulator Postures," *The International Journal of Robotics Research,* vol. 7, no. 5, pp. 13-21, 1988.

[10] Y. Wang and L. Wang, "Reactive Task-Oriented Redundancy Resolution Using Constraint-Based Programming," in *IEEE/RSJ International Conference on Intelligent Robots and Systems (IROS)*, Daejeon, Korea, 2016, pp. 5689-5694.

[11] R. Xu, J. Luo, and M. Wang, "Optimal grasping pose for dual-arm space robot cooperative manipulation based on global manipulability," *Acta Astronautica,* vol. 183, pp. 300-309, 2021.

[12] N. Vahrenkamp and T. Asfour, "Representing the robot's workspace through constrained manipulability analysis," *Autonomous Robots,* vol. 38, no. 1, pp. 17-30, 2014.

[13] R. Finotello, T. Grasso, G. Rossi, and A. Terribile, "Computation of Kinetostatic Performances of Robot Manipulators with Polytopes," in *IEEE International Conference on Robotics and Automation (ICRA)*, Leuven, Belgium, 1998, vol. 4, pp. 3241-3246.

[14] P. Long, T. Keleştemur, A. Ö. Önol, and T. Padir, "Optimization-Based Human-in-The-Loop Manipulation Using Joint Space Polytopes," in *IEEE International Conference on Robotics and Automation (ICRA)*, Montreal, Canada, 2019, pp. 204-210.

[15] M. Zolotas, M. Wonsick, P. Long, and T. Padir, "Motion Polytopes in Virtual Reality for Shared Control in Remote Manipulation Applications," *Front Robot AI,* vol. 8, p. 730433, 2021.

[16] Z. Wu, H. Yang, X. Liu, and K. Xu, "Dimension Reduced Instantaneous Inverse Kinematics for Configuration Variable Limits of Continuum Manipulators," in *IEEE International Conference on Robotics and Biomimetics (ROBIO)*, Dali, Yunnan, China, Dec 6-8 2019, pp. 303-308.

[17] K. L. Doty, C. Melchiorri, E. M. Schwartz, and C. Bonivento, "Robot Manipulability," *IEEE Transactions on Robotics and Automation,* vol. 11, no. 3, pp. 462 - 468, June 1995.

[18] D. N. Nenchev, "Restricted Jacobian Matrices of Redundant Manipulators in Constrained Motion Tasks," *The International Journal of Robotics Research,* vol. 11, no. 6, pp. 584-597, 1992.